

# Direct Evidence of Apex–Hypha Interactions During Vegetative Growth of Fungal Thallus via Comprehensive Network and Trajectory Extraction

Thibault Chassereau<sup>1</sup>, Florence Chapeland-Leclerc<sup>2</sup>, and Éric Herbert<sup>1,\*</sup>

<sup>1</sup>Université Paris Cité, CNRS, UMR 8236-LIED, F-75013 Paris, France

<sup>2</sup>Université Paris Cité, CNRS, UMR 8038-CiTCoM, F-75006 Paris, France

\*Corresponding author : eric.herbert@u-paris.fr

July 10, 2025

## Abstract

The mycelium of a filamentous fungus is a growing, branching network of numerous entangled hyphae exhibiting polarised apical growth. Expansion occurs during the vegetative phase from a single ascospore, driven by the need to explore and occupy surrounding space—limiting competitors, enhancing nutrient uptake, and promoting spore dispersal. Radial, rapid, and rectilinear growth combined with frequent branching appears adaptive. However, passive growth without interactions or feedback may produce suboptimal networks, as neither local density nor potential connectivity is considered. Reorientations of the apex near existing hyphae suggest apex–hypha feedback. Yet, the diversity of behaviours, spontaneous fluctuations, and limited apical trajectories studied leave open the question of active regulation. To investigate possible apex–hypha interactions, we analyse a dataset of *Podospora anserina* thallus growth by reconstructing all apical trajectories post-branching and fitting them with a classical Langevin model that incorporates potential interactions. Comparing isolated and non-isolated hyphae trajectories allows to identify a clear signature of interaction composed of abrupt deceleration and reorientation. This work opens the path towards a systematic exploration of hyphal interactions.

**Keywords:** network, growth, branching, morphogenesis, mycelium, hyphae, interactions, obstacles

## 1 Introduction

The growth of spatial branching networks is currently the focus of intense scientific investigation, largely driven by the emergence of new experimental setups that allow for time-lapse imaging of developmental dynamics such as root system [16] or blood network [20]. This allows for the development of reconstruction methods aimed at interpreting networks lacking growth time-lapse recordings, *eg* urban road network

[15] very slowly growing networks such as gorgonians. Among such systems, filamentous fungi [22, 12, 10, 7] are of particular interest, as they exhibit the key characteristics of branching networks: continuous growth, structural persistence, branching behavior, and the formation of anastomoses. A central question in understanding the architecture of these networks concerns their capacity for self-interaction—that is, the ability to adapt growth patterns in response to the proximity of other parts of the same network. This may involve, for instance, self-avoidance to optimize biomass distribution, or self-attraction to enhance internal connectivity.

The thallus of filamentous fungi, also known as mycelium, is a typical case for growing and branching networks. It consists of a series of interconnected hyphae, long cylinders from 2 to 20  $\mu\text{m}$  in diameter, which extend at their tip (or apex) [5]. Each apex eventually branches, giving rise to new apexes [3]. The ensemble of hyphae then forms a complex, dynamic living network, whose evolution is determined by the individual behavior of each hypha and by the arrangement of these filaments among themselves [9]. Then, the fungal network allows an efficient spatial exploration and exploitation of the nutritive resources and provides an effective response to external constraints disturbing their environmental exploration, which largely explains why these organisms occupy a much broader spectrum of habitats [8].

The phenomenon of autotropism between hyphae plays a key role in the overall organization of the mycelium. Negative autotropism describes the repulsive influence of hyphae on each other, whereas positive autotropism, by which hyphae attract each other, can lead to fusion, or anastomosis, particularly in ascomycetes and basidiomycetes [4]. Autotropism has been reported as intermittent, sometimes positive, sometimes negative, and often intertwined with other mechanisms—most notably spontaneous hyphal curvature—making its direct identification inherently challenging. To our knowledge, studies on autotropism

have relied on manually collected, isolated events that are prone to selection bias, and have never been conducted within the context of a complete hyphal network, primarily due to experimental limitations.

## 2 Modelling

We are interested in modelling the growth of hyphae forming the thallus of a filamentous fungus on a homogeneous and isotropic culture medium on a flat surface. The hyphae grow at their apex, whose displacement forms a trajectory. Experimentally, we observe apex trajectory over time to be largely rectilinear, with noise of biological origin, linked to the position of the Spitzenkörper (SPK) [1, 6]. A usual method for modelling this type of trajectory is to build on a Langevin equation that combines the effect of a drag force  $\gamma \mathbf{v}$  ( $1/\gamma$  is the timescale of the system) and a random forces  $\boldsymbol{\eta}$ :

$$\frac{d\mathbf{v}}{dt} = \mathbf{F}_g - \gamma \mathbf{v} + \boldsymbol{\eta} + \mathbf{I} \quad (1)$$

$\mathbf{F}_g$  correspond to the effective growth force. Its origin can be multiple (turgor pressure, osmotic pressure, etc.). We make the hypothesis that its norm is constant and that it is always aligned with the growth elongation vector  $\mathbf{v}$  as the tip of the hypha is softer than the rest of the cell. The term  $\gamma$  traduce the resistance by the medium and the limited capacity of the fungus to produce and transport to the SPK the material needed for the growth of the hyphae. The direction of hypha growth depends on the localisation of the Spitzenkörper, the term  $\boldsymbol{\eta}$  is there to represent the variable position of this vesicles cluster. We make the hypothesis that this relative position follows a 2D isotropic Gaussian noise without correlation in time. Moreover, the hyphae grows in a complex environment and can interact with eachother. The term  $\mathbf{I}$  is the result of all these contribution and should therefore be a function of time and spatial localization. The aim of this article is to distinguish the effect of interactions in the kinematics of growth. In a first step, we will focus in the case without interaction and therefore  $\mathbf{I} = \mathbf{0}$ . By projecting equation 1 into a Frenet frame ( $\mathbf{u}_v, \mathbf{u}_\theta$ ) centred on the apex ( $\mathbf{u}_v$  in the direction of  $\mathbf{v}$  and  $\mathbf{u}_\theta$  orthogonal), it follows that:

$$\begin{cases} \frac{dv}{dt} &= \gamma(v_\infty - v) + \eta_v \\ v \frac{d\theta}{dt} &= \eta_\theta \end{cases} \quad (2)$$

With  $v_\infty$  the apical asymptotic growth speed and  $\boldsymbol{\eta} = \eta_v \mathbf{u}_v + \eta_\theta \mathbf{u}_\theta$ . Under the assumption that  $\boldsymbol{\eta}$  is isotropic and follows a normal distribution centered at 0, with variance  $\sigma^2$  and without initial growth speed, it follows that  $\langle \theta \rangle = 0$  and  $\langle v \rangle$  time series can be written as:

$$\langle v \rangle = v_\infty (1 - \exp(-\gamma t)) \quad (3)$$

with  $\langle \cdot \rangle$  the ensemble average of  $(\cdot)$ . It is then straightforward to derive  $v_\infty$ :

$$v_\infty = \langle v \rangle + \frac{1}{\gamma} \left\langle \frac{dv}{dt} \right\rangle \quad (4)$$

Finally, by equating the variance of  $\eta_v$  and  $\eta_\theta$  in equations 2, and remember that  $v$  and  $\dot{v}$  are independent, *ie* the covariance vanishes, we can obtain the following expressions for  $\gamma$ :

$$\gamma = \sqrt{\frac{\langle v^2 \dot{\theta}^2 \rangle - \text{Var}(\dot{v})}{\text{Var}(v)}} \quad (5)$$

with  $\text{Var}(\cdot)$  the variance of  $(\cdot)$ .

Given the time series of  $v$  and  $\theta$  of non-interacting apex trajectories, it is then possible to estimate  $\gamma$ ,  $v_\infty$  and  $\sigma$ , allowing us to estimate  $\eta_v$  and  $\eta_\theta$  as respectively  $\frac{dv}{dt} - \gamma(v_\infty - v)$  and  $v \frac{d\theta}{dt}$ .

## 3 Results

Let-us now turn to the comparison with an experimental branching and growing network. We will build on the images of the 2-D growth of the thallus of saprophytic ascomycete filamentous fungi *Podospora anserina* obtained in the laboratory and described in [12, 17, 21] and in the appendix A.6 on homogeneous and isotropic medium. The time resolution is 18 min (see A.4 for a discussion). The comparison is based on five experiments described in [17]. The observed growths are initiated from a single ascospore and show, after a typical duration of 20 h, a dense network of several metres of hyphae and several thousands of branches.

A reconstruction of the network is then performed as shown in [21] to obtain the spatio-temporal graph of the entire thallus for the five experiments. The hyphae are reconstructed to take account of branches, anastomoses and crossings. For each hyphae of each thallus, the trajectory of the apex is reconstructed as the time series of the positions of the hyphal extremity, see blue lines in Fig. 1-A. We only consider the hyphae from an apical branching (see A.5).

Finally we constructed an interaction criterion based on the presence of a hypha near an apex, based on a conical-shaped detection area, see A.5 for details. Two-collections of apex trajectories are derived, one for which no interaction (named *free* hereafter) is expected and the second for which they are likely to exist (named *obstructed*). Figure 1-A illustrates the growth cone, with a free (green) and an obstructed case (red), and Table 1 for enumeration details.

Let-us now switch to the comparison with the model. From  $v$  and  $\theta$  time series we derived  $\gamma$ ,  $v_\infty$  and  $\sigma$ . Figure 1-B shows the superposition of the experimental velocities with the equation 3 parameterised with the values of  $\gamma$  and  $v_\infty$  obtained previously. The value of  $v_\infty \approx 300 \mu\text{m h}^{-1}$  is compatible with the ones reported in the literature for *P. anserina* [13] and with estimates previously obtained from the same thalli from manual [18] and automatic [21] extraction.

Except the initial short acceleration phase (approximately 1 hour), hyphae grow at a constant steady state speed as simplified in numerous previous models [2, 10]. In the permanent regime, the fluctuations of speed observed notably in [11] at higher temporal resolution,

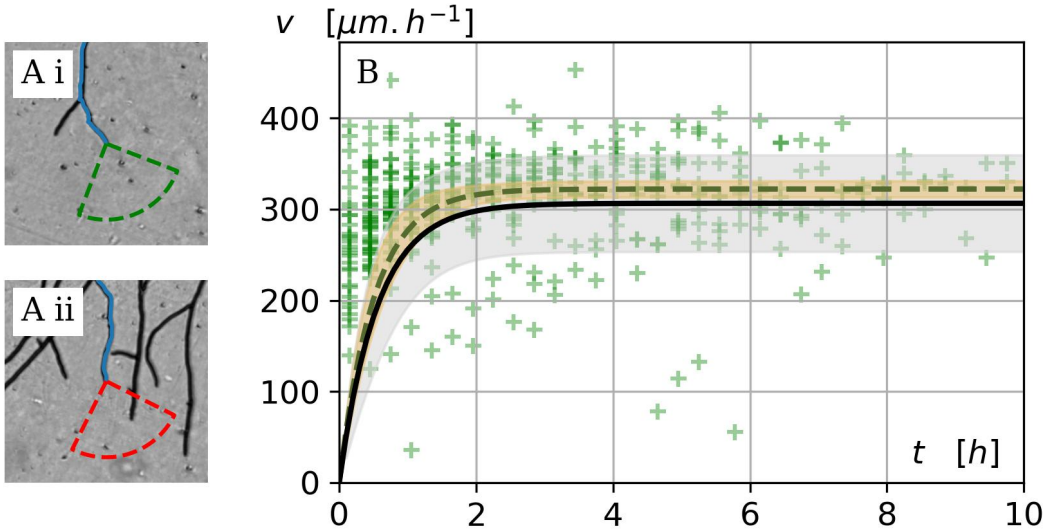


Figure 1: A) example of free (i) and obstructed (ii) field of growth on top of an apex. B) scatter plot of elongation speed as a function of time since the start of the growth of unobstructed apical branches for a network. Green dashed line correspond to the model evaluated on this network with green shade indicating 3 standard deviation estimated via bootstrap. Black line show the mean model over the 5 networks with the gray area showing 3 standard deviation.

with stops and slowdowns of growth of the mother hyphae at the time of a connection are averaged. The estimation of the acceleration term  $\gamma$  is found in agreement with [21].

The corresponding distributions (with expected  $\mathbf{I} = \mathbf{0}$ ) of  $\eta_v$  and  $\eta_\theta$  are shown figure 2-A. Results for the five networks are summarized in table 1. It corresponds to the 2D histogram of  $\eta_v = \frac{dv}{dt} - \gamma(v_\infty - v)$ , projection of  $\boldsymbol{\eta}$  in the growth direction, and of  $\eta_\theta = v \frac{d\theta}{dt}$ , projection of  $\boldsymbol{\eta}$  perpendicular to the growth direction.

$\sigma_\theta$  is estimated from the standard deviation  $\Sigma_\theta$  of  $\eta_\theta$  distribution corrected by the numerical error  $\epsilon_\theta$ :  $\sigma_\theta^2 = \Sigma_\theta^2 - \epsilon_\theta^2$ . Dashed circles centred at  $\mathbf{0}$  are of radius 1, 2 and 3  $\sigma_\theta$ . Projected distribution  $\eta_v$  and  $\eta_\theta$  are compared to the expected normal probability density function of mean 0 and of standard deviation  $\sigma_\theta$ . Each distribution of  $\eta_\theta$  is compatible with a normal law with standard deviation  $\sigma_\theta$ . Using Kolmogorov-Smirnov tests don't allow to distinguish the distribution of  $\eta_\theta$  from a normal distribution with the same mean and standard deviation with a p-value of 0.05. The mean of the observed distributions (at maximum  $25 \mu\text{m h}^{-2}$ ) is always smaller than the assumed error in the acceleration reading (of the order of  $56 \mu\text{m h}^{-2}$ . See the appendix A.4 for details. The distribution of  $\eta_v$  is found narrowed around 0 with more frequent rare events. This suggest that  $\eta_v$  doesn't follow a normal distribution and it is confirmed by Kolmogorov-Smirnov tests (p-value 0.99). Once the asymptotic speed is reached, the fluctuations are found to be indistinguishable from the experimental noise. It is known [11] that hyphae can undergo phases of acceleration interspersed with stationary phases. This phenomena could explain the more frequent extreme events seen in the distribution of  $\eta_v$ .

The model provides a satisfactory reproduction of the characteristic behaviour of free apical extension trajectories, *ie* without interaction. Let-us now move on to the second collection of apical extension trajectories with suspected interactions, for which  $\mathbf{I} \neq \mathbf{0}$  in equation 1. The part B of the figure 2 show the distribution of  $\boldsymbol{\eta} + \mathbf{I}$  for branches for which a section of thallus has been observed at least once in the growth cone. For comparison, we superimposed the centred normal distribution with standard deviation  $\sigma_\theta$  obtained in the case without interaction (dashed black lines).

It can be clearly seen that distribution is dramatically affected, both projections  $\eta_v + I_v$  and  $\eta_\theta + I_\theta$  are modified. In the direction of growth the distribution of  $\eta_v + I_v$  is almost uniformly spread out between  $-5\sigma$  and 0. This corresponds to deceleration events and can be interpreted as the consequence of rapid, large-scale reorientation. The distribution in the direction perpendicular to the growth of  $\eta_\theta + I_\theta$  is centred and symmetrical. This indicates that the reorientations are not biased in one direction (no chirality) and that they are brief, typically of the order of one time step. The distribution also appears to be narrower at zero. This suggest that, after an eventual initial change of direction, the growth direction is more constrained to the straight line by the interactions than it was in the case of unobstructed growth.

It is interesting to note that there is no global rotation effect, the mean is zero, and there are no abrupt reorientation events in both cases.

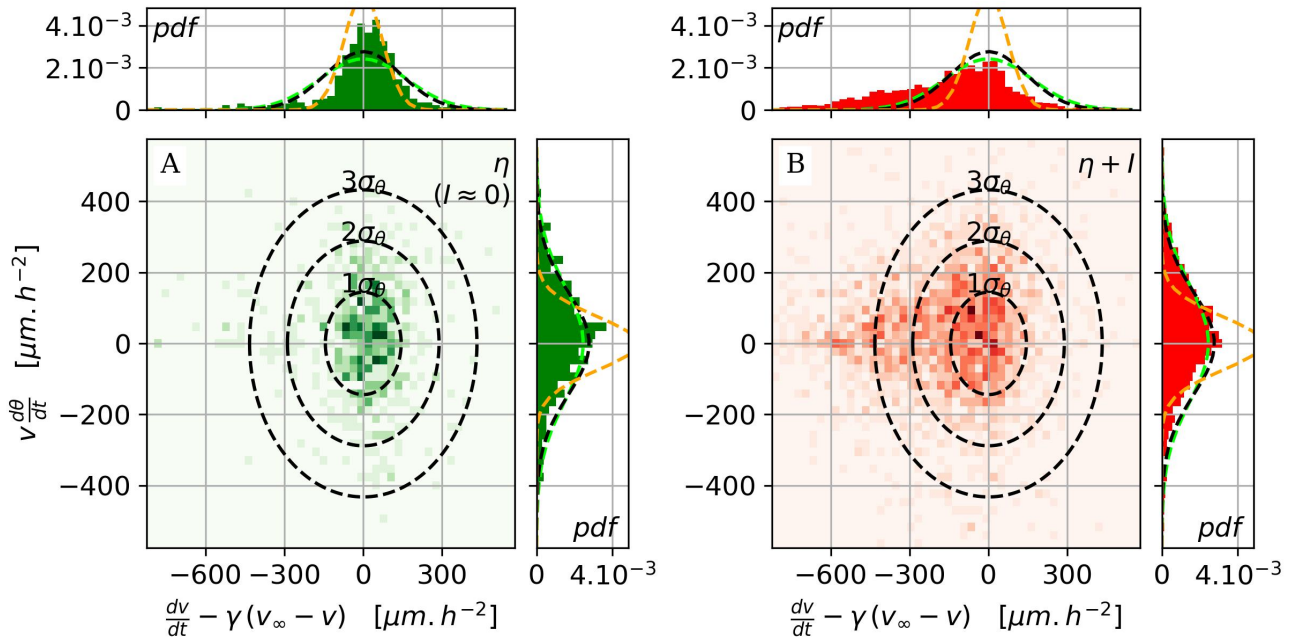


Figure 2: Example of 2D histograms  $\boldsymbol{\eta} + \boldsymbol{I}$  estimations made from the model for free branches (A), where  $\boldsymbol{I} = \mathbf{0}$ , and obstructed branches (B) for one of the five networks. Green dashed lines correspond to normal law centered at zero and of same standard deviation as the empirical distribution of free branches  $\Sigma$ ; orange dashed lines correspond to numerical error estimations  $\epsilon$ ; black dashed lines correspond to the normal law centered at zero and of standard deviation  $\sigma = \sqrt{\Sigma^2 - \epsilon^2}$ . All these lines are reported on the (B) side for comparison between free and obstructed branches.

Label	$N_{\text{free}}$	$n_{\text{free}}$	$N_{\text{obst}}$	$n_{\text{obst}}$	$\gamma$ [ $\text{h}^{-1}$ ]	$v_{\infty}$ [ $\mu\text{m h}^{-1}$ ]	$\Sigma_{\theta}$ [ $\mu\text{m h}^{-2}$ ]	$\sigma_{\theta}$ [ $\mu\text{m h}^{-2}$ ]
A	67	584	373	2 279	$1.8 \pm 0.2$	$317 \pm 4$	$163 \pm 7$	$144 \pm 5$
B	47	451	271	1 879	$2.0 \pm 0.2$	$322 \pm 3$	$139 \pm 8$	$105 \pm 6$
C	69	685	631	3 715	$2.2 \pm 0.2$	$322 \pm 3$	$150 \pm 4$	$133 \pm 5$
D	61	575	200	1 395	$1.5 \pm 0.2$	$280 \pm 3$	$129 \pm 5$	$105 \pm 5$
E	36	322	120	905	$1.5 \pm 0.2$	$291 \pm 5$	$126 \pm 6$	$101 \pm 6$
Mean $\pm$ s.d.	n.r.	n.r.	n.r.	n.r.	$1.8 \pm 0.3$	$307 \pm 18$	$141 \pm 14$	$118 \pm 17$

Table 1: Numerical details of the division of the population of apical branches into two sub-populations for each of the 5 networks A,B,C,D and E.  $n_{\text{free}}$  is the number of points extracted from  $N_{\text{free}}$  free apical branches while  $n_{\text{obst}}$  is the number of points extracted from  $N_{\text{obst}}$  obstructed apical. The corresponding numerical estimates of  $\gamma$ ,  $v_{\infty}$  and  $\Sigma_{\theta}$  are also given with the bootstrap estimated error. From the estimation of  $\Sigma_{\theta}$  we extract  $\sigma_{\theta}$  by correcting it from the estimated numerical error  $\epsilon_{\theta}$  (see text for more details)

## 4 Discussion and Conclusion

We propose a modelling of the trajectories of hyphal extension based on the well-known advection-diffusion equation, that combines a growing force  $\boldsymbol{F}_g$ , a friction force  $\gamma \boldsymbol{v}$ , a noise of biological origin  $\boldsymbol{\eta}$  and a force linked to self-interaction  $\boldsymbol{I}$ . This model satisfactorily reproduces the trajectories of freely moving apices, notably capturing the asymptotic velocity  $v_{\infty}$ , the initial acceleration  $\gamma$ , and the intensity of biological noise  $\sigma_{\theta}$ . The random force linked to the variation in the position of the SPK,  $\boldsymbol{\eta}$ , is about four times weaker than the growth force ( $\gamma v_{\infty} / \sigma_{\theta} \approx 4$ ), leading to observed trajectories that are largely rectilinear, with no chirality. We assumed that biological noise is isotropic; however, experimental observations reveal that only the fluctuations of  $\eta_{\theta}$  follow a Gaussian distribution centered at zero. In contrast, the distribution of  $\eta_v$  is both more

sharply peaked—due to the combined effects of numerical and biological noise around  $v_{\infty}$ —and exhibits heavy tails, reflecting the presence of extreme events associated with stop-and-go dynamics.

It then becomes possible to detect an effect of self-interaction. We find that this interaction leads to a statistically significant and pronounced reorientation of apical trajectories. The effect is both intense and short-lived, with the most prominent manifestation being a marked deceleration at the moment of reorientation.

Evidence of self-interaction implies a form of long-range communication enabling self-recognition during vegetative growth. Such an effect has also been observed in other species [4]. One explanation could be a chemotropism sensitive to a molecule produced by the apices during their growth. In [14] a modelling was proposed that takes into account diffusion of chemical species into the growing media to guide growth. To test

this hypothesis, it would be necessary to observe the correlation between reorientation, identification of the obstacle across the growth cone and the time elapsed since the obstacle grew at this point.

## References

- [1] Cristina G. Reynaga-Peña, Gerhard Gierz, and Salomon Bartnicki-Garcia. “Analysis of the role of the Spitzenkörper in fungal morphogenesis by computer simulation of apical branching in *Aspergillus niger*”. en. In: *Proceedings of the National Academy of Sciences* 94.17 (Aug. 1997), pp. 9096–9101. ISSN: 0027-8424, 1091-6490. DOI: [10.1073/pnas.94.17.9096](https://doi.org/10.1073/pnas.94.17.9096). URL: <https://pnas.org/doi/full/10.1073/pnas.94.17.9096> (visited on 04/11/2025).
- [2] I. Carver and Graeme Boswell. “A lattice-free model of translocation-induced outgrowth in fungal mycelia”. In: *IAENG International Journal of Applied Mathematics* 38 (Jan. 2008).
- [3] Graeme P. Boswell. “Modelling combat strategies in fungal mycelia”. en. In: *Journal of Theoretical Biology* 304 (July 2012), pp. 226–234. ISSN: 00225193. DOI: [10.1016/j.jtbi.2012.03.036](https://doi.org/10.1016/j.jtbi.2012.03.036). URL: <https://linkinghub.elsevier.com/retrieve/pii/S0022519312001683> (visited on 05/15/2025).
- [4] Anna Simonin et al. “Physiological Significance of Network Organization in Fungi”. In: *Eukaryotic Cell* 11.11 (Nov. 1, 2012). Publisher: American Society for Microbiology Journals Section: Articles, pp. 1345–1352. ISSN: 1535-9778, 1535-9786. DOI: [10.1128/EC.00213-12](https://doi.org/10.1128/EC.00213-12). URL: <https://ec.asm.org/content/11/11/1345> (visited on 07/20/2020).
- [5] Amir Sanati Nezhad and Anja Geitmann. “The cellular mechanics of an invasive lifestyle”. In: *Journal of Experimental Botany* 64.15 (Nov. 2013), pp. 4709–4728. ISSN: 1460-2431. DOI: [10.1093/jxb/ert254](https://doi.org/10.1093/jxb/ert254).
- [6] Meritxell Riquelme and Eddy Sánchez-León. “The Spitzenkörper: a choreographer of fungal growth and morphogenesis”. In: *Current Opinion in Microbiology* 20 (Aug. 2014), pp. 27–33. ISSN: 1879-0364. DOI: [10.1016/j.mib.2014.04.003](https://doi.org/10.1016/j.mib.2014.04.003).
- [7] Huan Du et al. “Morphological Characterization and Quantification of the Mycelial Growth of the Brown-Rot Fungus *Postia placenta* for Modeling Purposes”. In: *PLOS ONE* 11.9 (Sept. 7, 2016). Publisher: Public Library of Science, e0162469. ISSN: 1932-6203. DOI: [10.1371/journal.pone.0162469](https://doi.org/10.1371/journal.pone.0162469). URL: <https://journals.plos.org/plosone/article?id=10.1371/journal.pone.0162469> (visited on 07/07/2020).
- [8] Mark D. Fricker et al. “The Mycelium as a Network”. en. In: *Microbiology Spectrum* 5.3 (May 2017). Ed. by Joseph Heitman and Neil A. R. Gow, p. 5.3.03. ISSN: 2165-0497. DOI: [10.1128/microbiolspec.FUNK-0033-2017](https://doi.org/10.1128/microbiolspec.FUNK-0033-2017). URL: <https://journals.asm.org/doi/10.1128/microbiolspec.FUNK-0033-2017> (visited on 07/19/2024).
- [9] M. R. Islam et al. “Morphology and mechanics of fungal mycelium”. en. In: *Scientific Reports* 7.1 (Oct. 2017), p. 13070. ISSN: 2045-2322. DOI: [10.1038/s41598-017-13295-2](https://doi.org/10.1038/s41598-017-13295-2). URL: <https://www.nature.com/articles/s41598-017-13295-2> (visited on 08/26/2024).
- [10] G. Vidal-Diez de Ulzurrun et al. “Modelling three-dimensional fungal growth in response to environmental stimuli”. In: *Journal of Theoretical Biology* 414 (2017), pp. 35–49. ISSN: 0022-5193. DOI: [10.1016/j.jtbi.2016.11.020](https://doi.org/10.1016/j.jtbi.2016.11.020). URL: <https://www.sciencedirect.com/science/article/pii/S002251931630385X> (visited on 01/13/2022).
- [11] Gamaliel Sánchez-Orellana, Sergio Casas-Flores, and Braulio Gutiérrez-Medina. “Automated, continuous video microscopy tracking of hyphal growth”. In: *Fungal genetics and biology: FG & B* 123 (Nov. 30, 2018), pp. 25–32. ISSN: 1096-0937. DOI: [10.1016/j.fgb.2018.11.006](https://doi.org/10.1016/j.fgb.2018.11.006).
- [12] J. Dikec et al. “Hyphal network whole field imaging allows for accurate estimation of anastomosis rates and branching dynamics of the filamentous fungus *Podospora anserina*”. In: *Scientific Reports* 10.1 (Feb. 21, 2020), pp. 1–16. ISSN: 2045-2322. DOI: [10.1038/s41598-020-57808-y](https://doi.org/10.1038/s41598-020-57808-y). URL: <https://www.nature.com/articles/s41598-020-57808-y> (visited on 02/24/2020).
- [13] Philippe Silar. *Podospora anserina*. Feb. 2020. URL: <https://hal.science/hal-02475488>.
- [14] Manuella R. Clark-Cotton, Katherine C. Jacobs, and Daniel J. Lew. “Chemotropism and Cell-Cell Fusion in Fungi”. In: *Microbiol. Mol. Biol. Rev.* (Feb. 2022). URL: <https://journals.asm.org/doi/10.1128/membr.00165-21>.
- [15] Hanae El Gouj, Christian Rincón-Acosta, and Claire Lagesse. “Urban morphogenesis analysis based on geohistorical road data”. en. In: *Applied Network Science* 7.1 (Dec. 2022), p. 6. ISSN: 2364-8228. DOI: [10.1007/s41109-021-00440-0](https://doi.org/10.1007/s41109-021-00440-0). URL: <https://appliednetsci.springeropen.com/articles/10.1007/s41109-021-00440-0> (visited on 07/19/2024).
- [16] Romain Fernandez et al. “High-throughput and automatic structural and developmental root phenotyping on *Arabidopsis* seedlings”. en. In: *Plant Methods* 18.1 (Dec. 2022), p. 127. ISSN: 1746-4811. DOI: [10.1186/s13007-022-00960-5](https://doi.org/10.1186/s13007-022-00960-5). URL: <https://plantmethods.biomedcentral.com/articles/10.1186/s13007-022-00960-5> (visited on 08/23/2024).

- [17] Clara Ledoux. “Caractérisation multi-échelle de la dynamique de croissance d’un réseau fongique : étude du champignon filamenteux *Podospora anserina*”. fr. PhD thesis. 2023.
- [18] Clara Ledoux et al. “Prediction and experimental evidence of different growth phases of the *Podospora anserina* hyphal network”. In: *Scientific Reports* 13.1 (May 25, 2023). Number: 1 Publisher: Nature Publishing Group, p. 8501. ISSN: 2045-2322. DOI: [10.1038/s41598-023-35327-w](https://doi.org/10.1038/s41598-023-35327-w). URL: <https://www.nature.com/articles/s41598-023-35327-w> (visited on 05/30/2023).
- [19] Clara Ledoux et al. “Characterization of spatio-temporal dynamics of the constrained network of the filamentous fungus *Podospora anserina* using a geomatics-based approach”. In: *PLOS ONE* 19.2 (Feb. 6, 2024). Publisher: Public Library of Science, e0297816. ISSN: 1932-6203. DOI: [10.1371/journal.pone.0297816](https://doi.org/10.1371/journal.pone.0297816). URL: <https://journals.plos.org/plosone/article?id=10.1371/journal.pone.0297816> (visited on 02/07/2024).
- [20] Stanisław Żukowski et al. “Breakthrough-induced loop formation in evolving transport networks”. en. In: *Proceedings of the National Academy of Sciences* 121.29 (July 2024), e2401200121. ISSN: 0027-8424, 1091-6490. DOI: [10.1073/pnas.2401200121](https://doi.org/10.1073/pnas.2401200121). URL: <https://pnas.org/doi/10.1073/pnas.2401200121> (visited on 02/28/2025).
- [21] Thibault Chassereau, Florence Chapeland-Leclerc, and Eric Herbert. “Full identification of a growing and branching network’s spatio-temporal structures”. en. In: *Biophysical Journal* 124.2 (Jan. 2025), pp. 284–296. ISSN: 00063495. DOI: [10.1016/j.bpj.2024.12.002](https://doi.org/10.1016/j.bpj.2024.12.002). URL: <https://linkinghub.elsevier.com/retrieve/pii/S0006349524040633> (visited on 02/10/2025).
- [22] Loreto Oyarte Galvez et al. “A travelling-wave strategy for plant–fungal trade”. In: *Nature* 639.8053 (Mar. 2025). Publisher: Nature Publishing Group, pp. 172–180. ISSN: 1476-4687. DOI: [10.1038/s41586-025-08614-x](https://doi.org/10.1038/s41586-025-08614-x). URL: <https://www.nature.com/articles/s41586-025-08614-x> (visited on 04/04/2025).

## A Supplementary Material

### A.1 Data accessibility statement

Data and code are accessible through a [github](#) repository. Code is written in usual Python-3. A Jupyter Notebook is proposed that merges all the numerical work.

### A.2 Discretisation and estimation of growth elongation vectors

If we define the point  $A_i$  to be the  $i$ -th apex of a branch, at time  $t_i$ , at position  $(x_i, y_i)$  and corresponding to curvilinear abscissa  $s_i$  then we can define at the time  $\tilde{t}_i = \frac{t_i + t_{i+1}}{2}$  the following:

$$\begin{cases} v_i &= \frac{s_{i+1} - s_i}{\tilde{t}_{i+1} - \tilde{t}_i} \\ \theta_i &= \arctan\left(\frac{y_{i+1} - y_i}{x_{i+1} - x_i}\right) \\ \frac{dv}{dt} &= \frac{v_{i+1} - v_{i-1}}{(\tilde{t}_{i+2} + \tilde{t}_{i+1})/2 - (\tilde{t}_i + \tilde{t}_{i-1})/2} \\ \frac{d\theta}{dt} &= \frac{\theta_{i+1} - \theta_{i-1}}{(\tilde{t}_{i+2} + \tilde{t}_{i+1})/2 - (\tilde{t}_i + \tilde{t}_{i-1})/2} \end{cases} \quad (6)$$

where  $v$  corresponds to the norm of the growth vector,  $\theta$  to its orientation,  $\frac{dv}{dt}$  the change in the norm of the growth vector and  $\frac{d\theta}{dt}$  the change in its orientation.

### A.3 Propagation of measurement error

This section deals with the propagation of the error on the position of the apexes on the estimation of the  $\eta_v$  and  $\eta_\theta$  accelerations studied in the article. We assume that the error in position is the same in both directions of the plane and we denote it  $\delta x$ . Since the apparent diameter of hyphae is around  $10 \mu\text{m}$ , we estimate this uncertainty at a quarter of a hyphal diameter, i.e.  $3 \mu\text{m}$ . Considering that the two directions are independent, it follows that the error on  $\eta_v$ ,  $\delta\eta_v$  is equal to:

$$\delta\eta_v = \frac{2\delta x}{T^2} \sqrt{1 + \frac{\gamma^2 T^2}{2}} \quad (7)$$

and the error on  $\eta_\theta$  is equal to:

$$\delta\eta_\theta = \frac{2\delta x}{T^2} \sqrt{1 + \frac{\eta_\theta^2 T^2}{2v^2}} \quad (8)$$

where  $T = 18 \text{min}$  is time between 2 timesteps. In order to get a numerical estimation, we consider the case where  $\eta_\theta \approx \sigma \approx 150 \mu\text{m h}^{-2}$  and  $v \approx v_\infty \approx 300 \mu\text{m h}^{-1}$ . We then find  $\eta_\theta \approx 67 \mu\text{m h}^{-2}$ .

### A.4 Time resolution and numerical error.

If the delay between two images is too short then the error in the measurement will be too big to extract any information about the biological noise. At the opposite, if this delay is too large then we can only see an average version of what is really happening during the growth and we can miss on little variation.

To help us find a good compromise, we used a mycelial network of *P. anserina* that had grown under the same standard conditions but for which we had a time resolution of 4 min between each image. By subsampling this network we can measure the effect of the time resolution on the biological noise estimation.

In figure 3, we show the evolution of the characteristics (means  $\mu$  and standard deviations  $\Sigma$ ) of the empirical distributions of  $\eta_v$  and  $\eta_\theta$  as functions of the delay between consecutive images.

As predicted, a short time period between image leads to very large distributions as the numerical error is maximized. When the delay between images increase, the distributions converge toward the distribution of biological noise only as the numerical error decrease. After a 20-minute delay between two images, the benefits in terms of reducing digital noise are outweighed by the difficulty of reconstructing the growth of the network with any certainty. A good compromise was therefore found by taking a delay of 18 minutes between each image.

### A.5 Interaction criterion.

In the reconstruction, branches are automatically categorised as apical or lateral depending on the latency between the passage of the parent hypha and the appearance of the branch. Differences in the growth and location of the two kind of branches within the thallus have already been studied in the article [21], and we focus here on the apical branches. This is because we assume that interactions take place at short range and

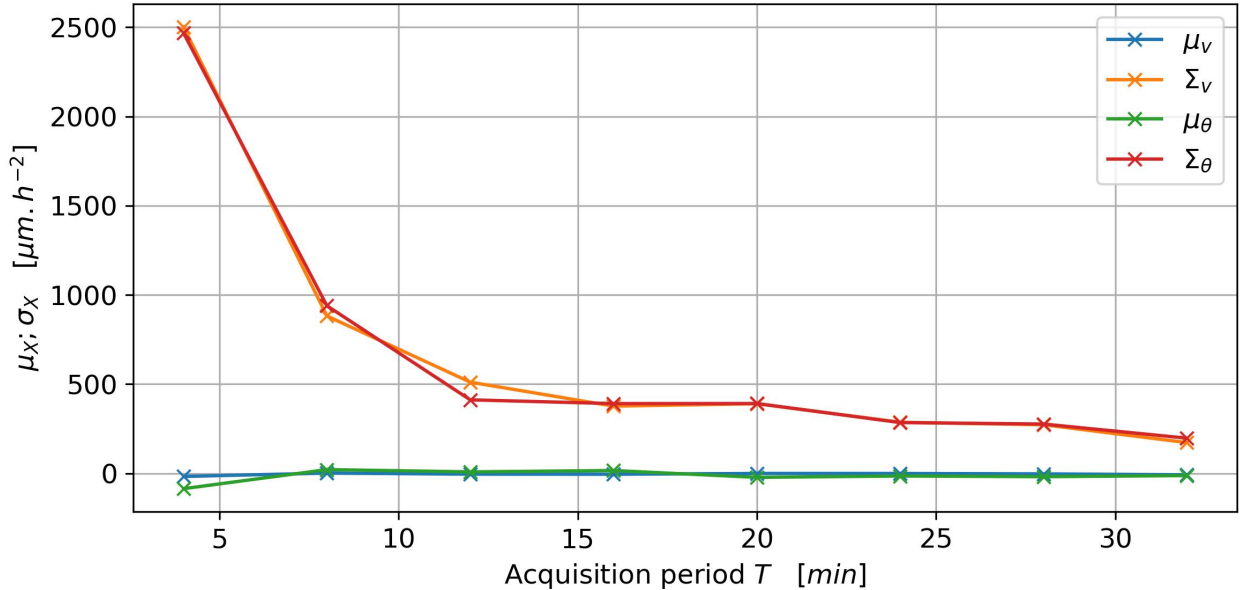


Figure 3: Characteristic (means  $\mu$  and standard deviations  $\Sigma$ ) of the distributions of  $\eta_v$  and  $\eta_\theta$  depending on the delay  $T$  between two consecutive images.

lateral branches appear exclusively within the thallus, in the densest zone. It is therefore difficult to extract a collection of non-interacting lateral branches to serve as a control population.

For this we use a cone centred on the apex and pointing in the direction of growth, of radius  $r = 180 \mu\text{m}$  and angle  $\alpha = \frac{\pi}{2}$ . The angle of the cone must not be too wide in order to avoid the inclusion of the parent branch at the time of branching, and its radius was chosen to be the length corresponding to the hyphal expansion during two time steps at asymptotic speed. At each time step, we checked that no element of the thallus was present in the cone. The collection of free hyphae (without interaction) never showed any presence in the cone, and the collection of non-free hyphae is complementary. Hyphae at the edge of the thallus are more likely to be non-interacting as they grow in a less dense region. The number of branches grows exponentially therefore the shortest hyphae are the most numerous. All the apices coming from an apical branching point, whose growth can be followed long enough to extract at least one acceleration vector, are used for each thallus. In order to extract 'stop and go' behavior [11] that could be misinterpreted as an interaction we remove branches that stop at least one time step. See table 1 for enumeration details.

## A.6 *Podospora anserina*

*Podospora anserina* is a saprophytic ascomycete filamentous fungus that makes an excellent laboratory model, in particular because its life cycle is short (around 7 days) and perfectly controlled in vitro on a standard culture medium [13]. In order to analyze the growth dynamics of *P. anserina* under controlled conditions, a two-dimensional image acquisition and processing system were developed in our laboratory a few years ago [12]. In particular, it has been used to characterize the behavior of a fungal thallus under various constraints [19] and to propose a complete identification of a growing and branching network's spatio-temporal structures thanks to a general method for global network reconstruction [21]. The reconstruction of the thallus as a spatio-temporal graph enables the individual tracking of all apices and the reconstruction of each growth trajectory. This yields a complete collection of apical trajectories, each associated with the position of the nearest hypha at every time point during growth. The dataset is divided into two subsets: the first corresponds to growth in the absence of nearby hyphae, allowing characterisation of velocity in a homogeneous and isotropic environment; the second includes potential interactions with neighbouring hyphae. These collections are subsequently compared to a stochastic growth model that incorporates both passive extension dynamics and active orientation mechanisms, with autotropism as a central component.